Supplementary Material

Supplement 1. The demonstrations of multi-model MRI preprocessing and features

Preprocessing of multi-modal MRI

For volumetric analysis of the structural MRI (sMRI), voxel-based morphometry was performed using the computational anatomy toolbox (CAT12). The images underwent denoising, bias cleaning, affine registration, segmentation, spatial normalization, volume modulation, and smoothing by full width at half maximum (FWHM) = 4 mm Gaussian kernel. Supplementary Figure 1 shows the segmented images of gray matter, white matter, and cerebrospinal fluid (CSF) of the same subject for the illustration of the spatial ranges of voxel-based morphometry (VBM).

For surface analysis of the sMRI, surface-based morphometry (SBM) was performed using CAT12 (1). Four surface metrics were extracted by a surface atlas (2): 1. The cortical thickness; 2. The gyrification index (GI) based on absolute mean cortical curvature; 3. The fractal dimension value (FD) based on the cortical complexity; 4. The sulcus depth (SD) based on the Euclidean distance between the central surface and its convex hull. All result metrics were resampled and smoothed by FWHM = 15 mm Gaussian kernel.

Rs-fMRI images were processed by Data Processing Assistant for Resting-State fMRI (DPARSF) v5.2 (3), which included steps of removing the first 10 time points, slice timing, realignment, affine registration, nuisance covariates regression, head motion correction, and spatial normalization. Fractional amplitude of low-frequency fluctuations (fALFF) (4), degree centrality (DC) and regional homogeneity (ReHo) (5) were calculated, voxel z-scored across each image, smoothed by FWHM = 4 mm Gaussian kernel.

Cerebral blood flow (CBF) was calculated from pseudocontinuous ASL perfusion images and proton-density–weighted (PD) images by locally created Matlab scripts, using the CBF quantification pipeline (6) and regression-based partial volume correction (7). PD and ASL images were coregistered with the corresponding T1-sMRI. CBF was calculated and corrected for the partial volume effect using the tissue

segmentation from T1-sMRI. We normalized the whole-brain CBF in voxels using the mean value of CBF in the whole-brain cerebrospinal fluid (CSF) regions to control for the potential individual and scanner variability.

Demonstrations of the MRI features

Among all the features used for prediction, the cortical thickness (CT), gyrification index (GI), fractal dimension (FD), and sulcus depth (SD) used for surface analysis, along with the fractional amplitude of low-frequency fluctuations (fALFF), regional homogeneity (ReHo), and degree centrality (DC), are common but indirect MRI measurements that need further clarification. We provided detailed demonstrations of these features:

1. Cortical thickness (CT): This measure refers to the thickness of the cortex in the brain.

2. Gyrification index (GI): A measure of the amount of folding on the surface of the brain (8). It is calculated as the ratio of the cortex within the sulcal folds against the outer visible cortex. A higher GI signifies more extensive brain folding.

3. Fractal dimension (FD): This measure quantifies how completely a fractal appears to fill space (9). In the context of the brain, it's a measure of the complexity of the cortical surface. The higher the FD, the more complex the cortex is.

4. Sulcus depth (SD): Sulcus are the grooves on the brain's surface. The depth of these sulci can be an important measure of brain morphology. Deeper sulci may suggest a larger surface area of the cortex hidden within these grooves.

5. Fractional amplitude of low-frequency fluctuations (fALFF): fALFF quantifies the relative contribution of low-frequency oscillations (typically in the range of 0.01–0.08 Hz) to the total power in the entire detectable frequency range of the blood oxygenation level dependent (BOLD) signal (4). Larger fALFF refers to greater spontaneous brain activity.

6. Regional homogeneity (ReHo): ReHo measures the similarity or synchronization of the time series of neighboring voxels (5). A higher ReHo value indicates greater local synchronization, suggesting that those brain regions are more functionally homogeneous or are working more closely together.

7. Degree centrality (DC): In graph theory, DC is the number of direct connections (or

edges) a node (or a brain region) has. In neuroscience, a higher DC for a brain region suggests that it's highly connected with other regions, implying that it may play a crucial role in brain communication and coordination.

Supplement 2. Details of prediction and statistical analysis implementation

Here we provided the implementation and choices of the prediction and statistical analysis for better reproducibility of results.

Choice of prediction inputs

For prediction inputs, we used 11 features from various MRI modalities, complemented with six sea-level demographic and physiological features: age, sex, body mass index, mean arterial pressure, heart rate, and saturation of pulse oxygen. Because we used both Anatomical Automatic Labeling (AAL) (10) and surface-specific Desikan-Killiany atlas (2), the total number of input features is 7×166+4×68+6=1440. However, to avoid overfitting and screen the valid predictors, we used each feature in the regions of interest (ROIs) as input separately for each prediction, such as 68 values of cortical thickness with six sea-level demographic and physiological features.

Least absolute shrinkage and selection operator (LASSO) logistic regression

In a general logistic model, where y is the label to predict, X is the potential predictors, and β is the coefficients estimated by the least square method:

$$y = logistic(X\beta)$$

Least absolute shrinkage and selection operator (LASSO) (11), also called L1-regulation, uses a penalty of β to select the most valid predictors while making the linear model convergent by:

$$\min_{\beta \in \mathbb{R}^p} \{\frac{1}{N}\|y - X\beta\|^2\} \ subject \ to \ \|\beta\|_1 < C$$

As a result, sparse coefficients were estimated, leaving only valid predictors as non-zero. We then considered these predictors, with non-zero coefficients in the LASSO cross-validation, as valid predictors for acute mountain sickness (AMS). In this study, we implemented LASSO by the logistic regression with L1-regulation in scikit-learn

toolbox and selected optimal C-value by cross-validation, which was addressed in the method part of manuscript.

Supplement 3. Detailsof acute mountain sickness diagnosis and study design

We listed the detailed acute mountain sickness (AMS) diagnosis list in Supplementary Table 1. For diagnosing AMS, we used the newest version of scoring system defined by Lake Louise Consensus Committee (12), in the standard form of self-report questionnaires. Participants with high-altitude headache (HAH) score $\geq$ 1 and Lake Louis Score (LLS) $\geq$ 3 were diagnosed as AMS on a daily basis. Participants that were at least once diagnosed among five days at high altitude were grouped as AMS. Participants that were never diagnosed as AMS were grouped as non-AMS.

Because all participants in this study were sea-level residents, our research does not encompass chronic mountain sickness, which is typically associated with natives or long-time residents of high-altitude area (13).

In this study, we believe that the potential confounding effect of flight travel on AMS is negligible due to: 1) Direct, short flights from Beijing to Lhasa (3-4 hours) cross only two time zones. Previous research (14) indicates jet lag is rare for such short flights. 2) Flights were scheduled during daytime, lessening the effect of sleep disruption, which was a key factor in jet lag. 3) Previous research (15) suggests that the effects of high-altitude exposure during flight do not significantly influence the diagnostic criteria for AMS. These factors contribute to the study's robustness and accurate on the AMS diagnosis regardless of potential flight effect.

In Lhasa, participants were allowed to freely sightsee only within the city area and were not allowed for any intensive physical activities including long-distance walking. They were also prohibited from consuming any food or beverages containing alcohol or caffeine. They ate and drank according to their personal needs, without any regulation to increase or restrict the quantity.

Supplement 4. Detailed prediction performance of all kinds of inputs

We listed the predicting performance of all kinds of features as inputs in Supplementary Table 2. Additionally, in Supplementary Figure 2, we have illustrated all the ROC curves for the predictions listed in Supplementary Table 2. For each ROC curve, we have marked the optimal cut point determined by Youden's index, along with their coordinates (1-specificity, sensitivity). The table includes single types of features such as gray matter volume (GMV) or cortical thickness (CT), as well as combined features like all the fMRI metrics or all the MRI metrics. The results showed that only fractional amplitude of low-frequency fluctuations (fALFF) and degree centrality (DC) had significant predictive power when used as single input features. However, when these features were combined, they did not show any significant predictive power.

Supplement 5. Verifying valid predictors by cross-validation and varying LASSO parameters

These predictors selected by LASSO models remained robust during the 45 iterations of leave-one-out cross-validation, as shown in the heatmap of coefficients in Supplementary Figure 3. The major predictors consistently had non-zero coefficients, even in different training/testing sets of cross-validation.

To ensure that the selected important features with significant coefficients in L1-regulated logistic regression were not specialized to the sparsity strength of coefficient, we listed the coefficient range with C-value varying from 0.2 to 1 (step = 0.01) for all input features, in the valid prediction of DC and fALFF inputs (Supplementary Figure 4). As a result, the coefficients of the important features in Table 3 of the main manuscript showed consistency across different sparsity strengths.

Supplement 6. Correlation analysis between multi-modal MRI at high altitude

By using the multi-modal MRI scanned at 22 hours at high altitude, we further identified the influence of fMRI predictors (fALFF and DC) by performing Partial Pearson's correlation between fMRI predictors and other modalities of brain MRI (the whole brain gray matter volume, white matter volume, cerebrospinal fluid volume, and cerebral blood flow). The complete results are shown in Supplementary Table 3.

Notably, the correlation between cerebrospinal fluid volume (CSFV) and fALFF in the somatomotor network (SMN) was significantly different from zero, as determined by the t-test.

Supplement 7. VBM analysis of CSF changes

Regarding the localized differences in CSF changes between sea level and high-altitude, we performed paired t-tests among 45 participants on the VBM images of CSF, the results is shown in Supplementary Figure 5 below. We found that CSF were significantly increased in both intraventricular and cisternal spaces, under a strict threshold of family-wise error (FWE) corrected $P < 0.05$. The main regions of CSF increase include the lateral, third, fourth ventricles, and the interhemispheric cistern. As a result, in brief, we found no significant localized difference in CSF volume change but observed a widespread range of CSF changes in a strict P-value threshold.

Supplement 8. Longitudinal analysis of oxygen saturation

We provide a detailed analysis of the oxygenation status recorded at various time points during our study (see supplementary Figure 6). The time points for these measurements were strategically chosen to encompass the period before exposure to high altitude, as well as several critical periods following exposure: 9 hours, 22 hours, 46 hours, 70 hours, and 94 hours post-exposure. These time frames were selected to capture the acute physiological responses as well as any delayed effects that might occur due to high altitude exposure.

Reference for Supplementary Material

1. Yotter RA, Dahnke R, Thompson PM, Gaser C. Topological correction of brain surface meshes using spherical harmonics. Human Brain Mapping. 2011;32(7):1109–24.

2. Desikan RS, Segonne F, Fischl B, Quinn BT, Dickerson BC, Blacker D, et al. An automated labeling system for subdividing the human cerebral cortex on MRI scans into gyral based regions of interest. Neuroimage. 2006 Jul 1;31(3):968–80.

3. Chao-Gan Y, Yu-Feng Z. DPARSF: A MATLAB Toolbox for "Pipeline" Data Analysis of Resting-State fMRI. Frontiers in systems neuroscience. 2010;4:13–13.

4. Zou QH, Zhu CZ, Yang Y, Zuo XN, Long XY, Cao QJ, et al. An improved approach to detection of amplitude of low-frequency fluctuation (ALFF) for resting-state fMRI: Fractional ALFF. Journal of Neuroscience Methods. 2008 Jul 15;172(1):137–41.

5. Zang YF, Jiang TZ, Lu YL, He Y, Tian LX. Regional homogeneity approach to fMRI data analysis. Neuroimage. 2004 May;22(1):394–400.

6. Lehmann P, Monet P, de Marco G, Saliou G, Perrin M, Stoquart-Elsankari S, et al. A Comparative Study of Perfusion Measurement in Brain Tumours at 3 Tesla MR: Arterial Spin Labeling versus Dynamic Susceptibility Contrast-Enhanced MRI. European Neurology. 2010;64(1):21–6.

7. Asllani I, Borogovac A, Brown TR. Regression algorithm correcting for partial volume effects in arterial spin labeling MRI. Magn Reson Med. 2008 Dec;60(6):1362–71.

8. Schaer M, Cuadra MB, Tamarit L, Lazeyras F, Eliez S, Thiran JP. A surface-based approach to quantify local cortical gyrification. IEEE transactions on medical imaging. 2008;27(2):161–70.

9. Im K, Lee JM, Yoon U, Shin YW, Hong SB, Kim IY, et al. Fractal dimension in human cortical surface: multiple regression analysis with cortical thickness, sulcal depth, and folding area. Human brain mapping. 2006;27(12):994–1003.

10. Rolls ET, Huang CC, Lin CP, Feng J, Joliot M. Automated anatomical labelling atlas 3. NeuroImage. 2020 Feb;206:116189.

11. Tibshirani R. Regression shrinkage and selection via the lasso. Journal of the Royal Statistical Society: Series B (Methodological). 1996;58(1):267–88.

12. Roach RC, Hackett PH, Oelz O, Baertsch P, Luks AM, MacInnis MJ, et al. The 2018 Lake Louise Acute Mountain Sickness Score. High Altitude Medicine & Biology. 2018 Mar;19(1):4–6.

13. León-Velarde F, Maggiorini M, Reeves JT, Aldashev A, Asmus I, Bernardi L, et al. Consensus Statement on Chronic and Subacute High Altitude Diseases. High Altitude Medicine & Biology. 2005 Jun;6(2):147–57.

14. Sack RL. Jet Lag. N Engl J Med. 2010 Feb 4;362(5):440–7.

15. Muhm JM, Rock PB, McMullin DL, Jones SP, Lu IL, Eilers KD, et al. Effect of Aircraft-Cabin Altitude on Passenger Discomfort. New England Journal of Medicine. 2007 Jul 5;357(1):18–27.

Supplementary Table 1. Detailed AMS diagnosis list. Positive diagnoses were bold.

Participant No.	HAH D1	LLS D1	HAH D2	LLS D2	HAH D3	LLS D3	HAH D4	LLS D4	HAH D5	LLS D5	AMS or not
1	**1**	**4**	0	0	0	0	0	0	0	0	**1**
2	**1**	**4**	**1**	**4**	**2**	**5**	**1**	**4**	**1**	**4**	**1**
3	**1**	**5**	**2**	**8**	**2**	**8**	**1**	**5**	0	2	**1**
4	**1**	**10**	**1**	**5**	0	2	0	3	**1**	**4**	**1**
5	0	3	**1**	**4**	**1**	**5**	0	2	0	3	**1**
6	1	1	0	0	1	1	**1**	**4**	1	1	**1**
7	1	1	0	1	0	1	0	2	0	0	0
8	1	2	0	1	0	1	0	1	0	2	0
9	**1**	**4**	**1**	**3**	0	0	**2**	**4**	0	0	**1**
10	**1**	**8**	**1**	**4**	**1**	**5**	**1**	**3**	**2**	**3**	**1**
11	**1**	**4**	**1**	**7**	**1**	**4**	**1**	**4**	**1**	**4**	**1**
12	**1**	**3**	**1**	**4**	**1**	**3**	**1**	**3**	0	2	**1**
13	**1**	**4**	0	2	**2**	**5**	**1**	**3**	0	2	**1**
14	1	2	1	2	0	0	0	0	0	0	0
15	0	4	**1**	**4**	**1**	**4**	0	3	0	3	**1**
16	**2**	**6**	**2**	**6**	**1**	**4**	**1**	**4**	1	2	**1**
17	**1**	**4**	0	2	1	2	0	0	0	0	**1**
18	0	1	0	2	0	1	0	1	0	0	0
19	**1**	**5**	0	3	**1**	**4**	0	2	**1**	**4**	**1**
20	0	0	0	0	0	0	0	0	0	0	0
21	0	0	0	0	0	0	0	0	0	0	0
22	0	3	0	0	**1**	**4**	0	0	**1**	**3**	**1**
23	**1**	**4**	**1**	**4**	**1**	**4**	**1**	**4**	0	3	**1**
24	1	2	1	2	1	2	0	2	0	0	0
25	**1**	**11**	0	2	**1**	**4**	0	0	0	0	**1**
26	**1**	**4**	**1**	**4**	**1**	**4**	**1**	**4**	0	0	**1**
27	**1**	**8**	**1**	**8**	0	2	0	0	0	0	**1**
28	**1**	**3**	1	2	0	1	0	0	1	2	**1**
29	**1**	**3**	**1**	**7**	0	2	0	0	0	1	**1**
30	0	3	0	3	**1**	**6**	0	5	**1**	**5**	**1**
31	**1**	**3**	0	1	0	1	0	0	0	0	**1**
32	**1**	**4**	**1**	**4**	**1**	**3**	**1**	**3**	0	1	**1**
33	**1**	**4**	**2**	**7**	1	2	0	0	0	1	**1**
34	**1**	**3**	**1**	**3**	0	0	0	0	0	0	**1**
35	1	1	1	2	**3**	**8**	0	0	0	0	**1**
36	**2**	**7**	**2**	**8**	**2**	**7**	**1**	**6**	**1**	**6**	**1**
37	**1**	**5**	**2**	**7**	0	2	0	2	0	4	**1**
38	**2**	**9**	**2**	**9**	**2**	**11**	**1**	**7**	**2**	**9**	**1**
39	**1**	**3**	**1**	**3**	0	1	0	1	0	0	**1**
40	**1**	**3**	0	1	0	0	0	0	0	0	**1**
41	**1**	**4**	0	1	**1**	**3**	0	1	0	1	**1**
42	**3**	**12**	**2**	**10**	**3**	**10**	**1**	**3**	0	1	**1**
43	**2**	**6**	**2**	**4**	**1**	**3**	0	2	0	2	**1**
44	0	2	0	2	0	0	0	0	0	0	0
45	0	1	0	1	0	1	0	1	0	0	0

Abbreviations: D = day No.; HAH = high-altitude headache; LLS = Lake Louis Score

Supplementary Table 2. Predicting performance by the area under curve (AUC) of receiver operation curve (ROC) for different input types. Significant inputs are bold.

| Modalities	Features	AUC	Std of AUC	Lower 95% CI	Upper 95% CI	P-value	Sensitivity	Specificity	Youden Index
T1-sMRI (volume)	Gray matter volume (GMV)	36.7%	9.0%	19.1%	54.4%	0.2224	30.6%	77.8%	0.084
	White matter volume (WMV)	60.5%	10.2%	40.5%	80.5%	0.3347	77.8%	55.6%	0.334
	Cerebrospinal fluid volume (CSFV)	47.5%	12.4%	23.3%	71.8%	0.8204	58.3%	55.6%	0.139
	3 features combined	37.0%	8.7%	19.9%	54.1%	0.2334	19.4%	88.9%	0.083
T1-sMRI (surface)	Cortical thickness (CT)	29.0%	12.2%	5.2%	52.8%	0.0537	72.2%	33.3%	0.055
	Gyrification index (GI)	71.3%	10.3%	51.1%	91.5%	0.0502	66.7%	88.9%	0.556
	Fractal dimension (FD)	19.4%	7.6%	4.6%	34.3%	0.0050	100.0%	0.0%	0.000
	Sulcus depth (SD)	43.8%	12.6%	19.1%	68.6%	0.5704	86.1%	33.3%	0.194
	4 features combined	55.3%	11.2%	33.4%	77.1%	0.6295	52.8%	66.7%	0.195
Rs-fMRI	**Fractional amplitude of low-frequency fluctuations (fALFF)**	**78.1%**	**8.0%**	**62.4%**	**93.8%**	**0.0098**	80.5%	77.8%	0.583
	Regional homogeneity (ReHo)	60.5%	9.5%	41.8%	79.2%	0.3347	58.3%	77.8%	0.361
	Degree centrality (DC)	**86.4%**	**5.4%**	**75.9%**	**96.9%**	**0.0008**	77.8%	100.0%	0.778
	3 features combined	54.0%	10.5%	33.4%	74.6%	0.7122	58.3%	77.8%	0.361
Arterial spin labeling (ASL)	Cerebral blood flow (CBF)	54.9%	10.1%	35.1%	74.8%	0.6498	47.2%	77.8%	0.250
ALL MRI images	11 features combined	47.8%	10.8%	26.7%	68.9%	0.8426	50.0%	66.7%	0.167

Supplementary Table 3. Partial Pearson's correlation analyses between fMRI predictors and brain features from other MRI modalities. Correlations were shown in the format of $r$ho (P-value). Note that all features were measure at 22 hours at high altitude, and Δ refers to changes between high altitude and sea level.

	ΔGMV	ΔWMV	ΔCSFV	ΔCBF
fALFF in SMN	-0.1522 (0.3422)	0.0489 (0.7614)	0.3277 (0.0365)	0.1184 (0.4611)
DC in SMN	-0.0948 (0.5554)	-0.0526 (0.7438)	0.0500 (0.7564)	0.0061 (0.9698)

Abbreviations: ΔGMV = change in gray matter volume; ΔWMV = change in white matter volume; ΔCSFV = change in cerebrospinal fluid volume; ΔCBF = change in cerebral blood flow; fALFF in SMN = fractional amplitude of low frequency fluctuations in somatomotor network; DC in SMN = degree centrality in somatomotor network.

Supplementary Figure 1. Voxel-based morphometry (VBM) analysis showing segmented images of gray matter, white matter, and cerebrospinal fluid (CSF) of the same subject for the illustration of the spatial ranges of VBM.
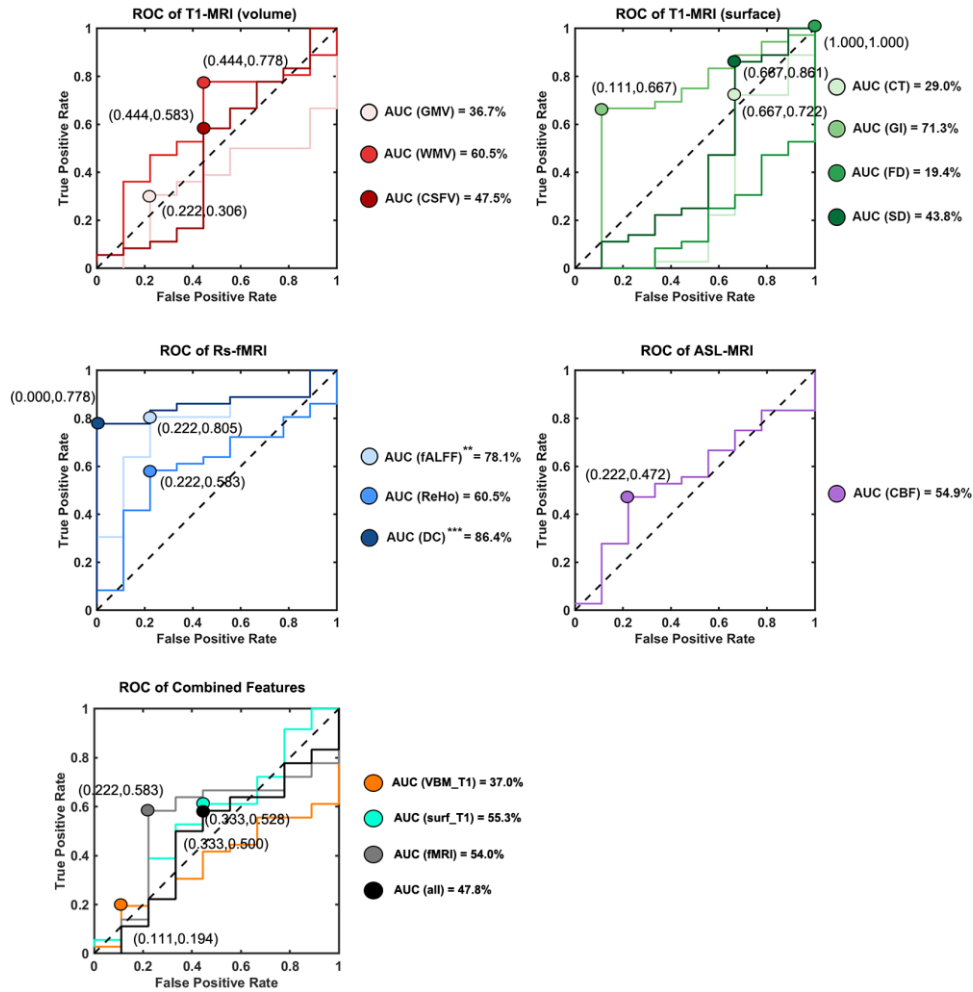
Supplementary Figure 2. Receiver operator characteristic (ROC) curve analysis of MRI features' predictive performance, marking cut points where Youden's index is optimized to define sensitivity and specificity. The prediction performance using different features of multi-modal MRI as inputs, measured by the area under curve (AUC) of the ROC curves. Fractional amplitude of low-frequency fluctuations (fALFF) and degree centrality (DC) from fMRI were detected as valid predictors, yielding significant AUC values. **: $P < 0.01$; ***: $P < 0.001$.

Abbreviations: CBF = cerebral blood flow, CSFV = cerebrospinal fluid volume, CT = cortical thickness, DC = degree centrality, FD = fractal dimension, fALFF = fractional amplitude of low-frequency fluctuations, GI = gyrification index, GMV = gray matter volume, ReHo = regional homogeneity, SD = sulcus depth, surf = surface analysis, VBM = voxel-based morphometry, WMV = white matter volume
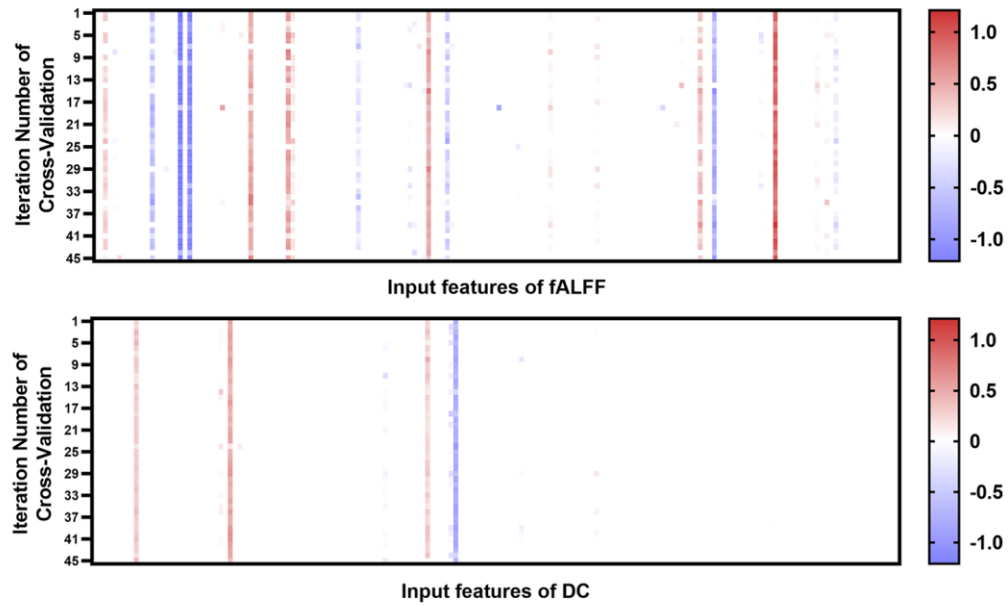
Supplementary Figure 3. Heatmaps displaying the standardized coefficients from the LASSO-LR during 45 iterations of leave-one-out cross-validation. Coefficients represent the significance of the predictors, which are consistent across iterations. The top panel reflects the input features of fractional amplitude of low-frequency fluctuations (fALFF), while the bottom panel shows the input features of degree centrality (DC).
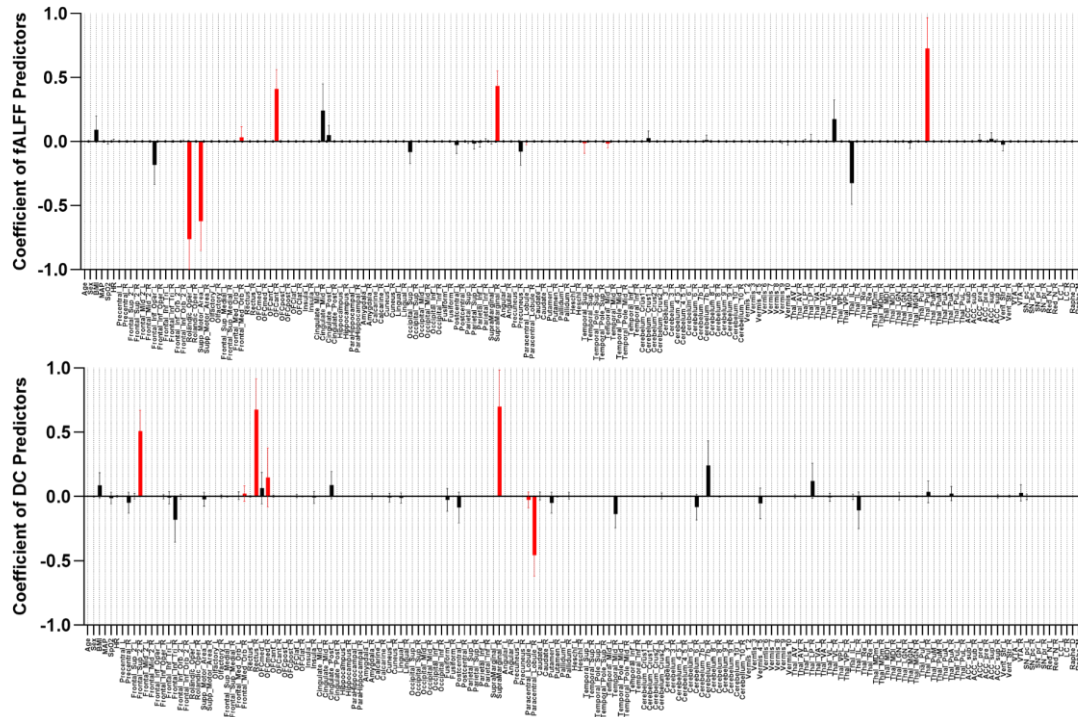
Supplementary Figure 4. Coefficient ranges with standard deviations for prediction models using the inputs of fractional amplitude of low-frequency fluctuations (fALFF) and degree centrality (DC). Valid predictors listed in Table 3 are marked in red. These ranges encompass all models using the least absolute shrinkage and selection operator (LASSO) across different cross-validation sets and various hyperparameter choices of C-value.
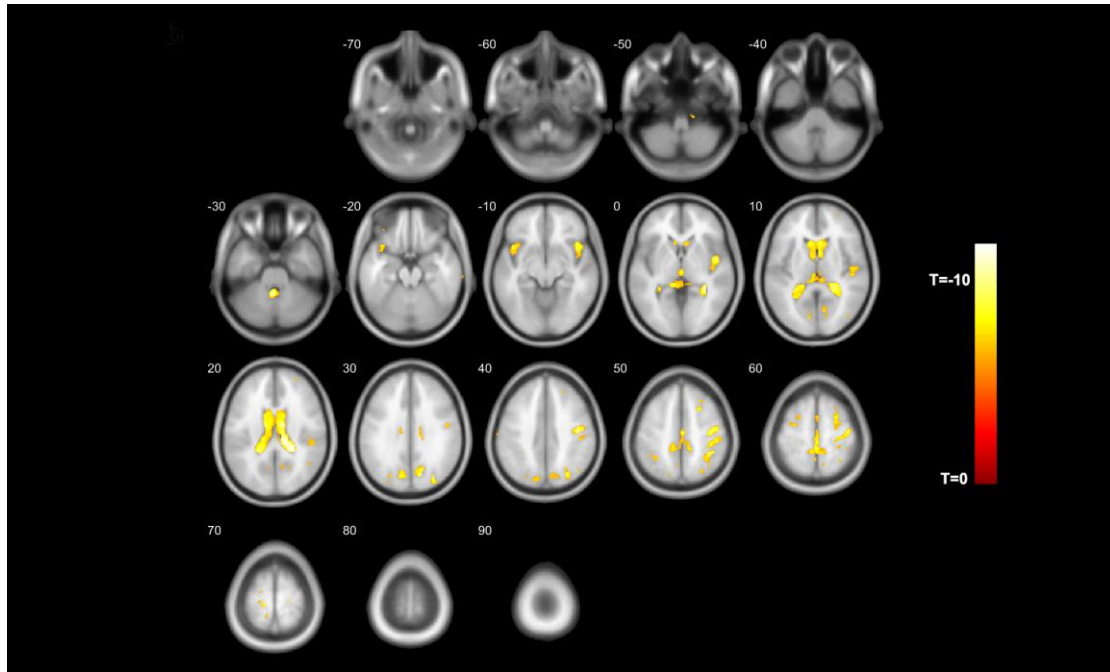
Supplementary Figure 5. Significant changes of cerebrospinal fluid (CSF) after high-altitude exposure, measured by paired T-tests on 45 participants, using threshold of family-wise error (FWE) corrected $P < 0.05$.
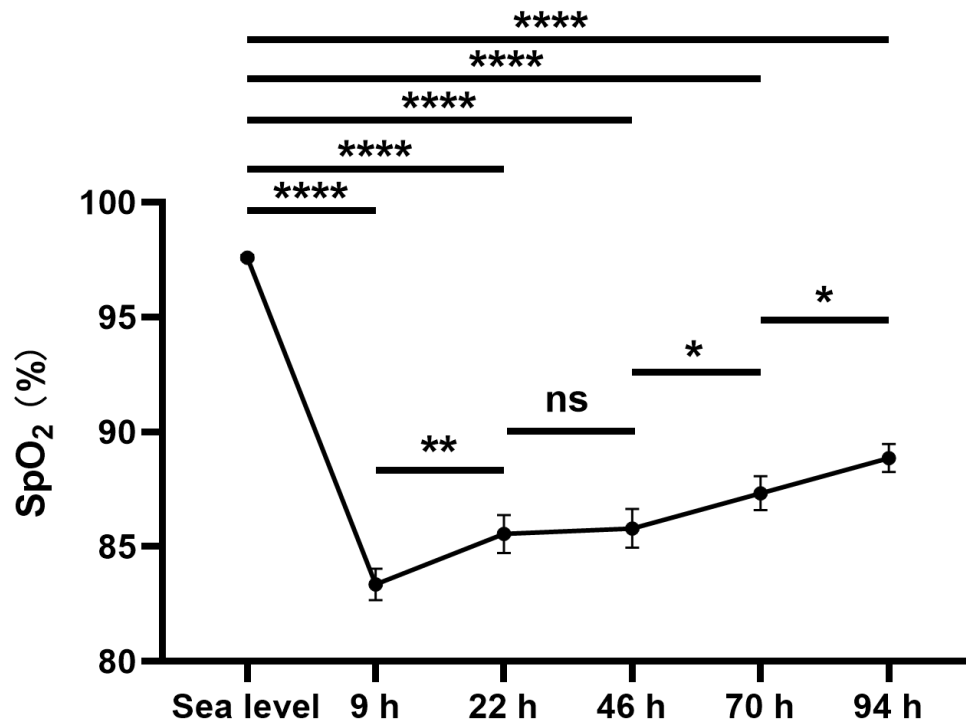
Supplementary Figure 6. Measurement of blood oxygen saturation (SpO_2) in 45 participants before and after high altitude exposure. Changes at different time points were assessed using paired T-tests (*: $P < 0.05$, **: $P < 0.01$, ****: $P < 0.0001$, ns = not significant). Error bar refers to standard error of the mean (SEM).